Bidirectional Photoinduced Energy Transfer in Nanoassemblies of Quantum Dots and Luminescent Metal Complexes

Srinidhi Ramachandra[a], Cristian Alejandro Strassert[b], David N. Reinhoudt[a], Daniel Vanmaekelbergh[c], and Luisa De Cola[a,b,d]

[a] Laboratory of Supramolecular Chemistry and Technology, and MESA+ Institute of Nanotechnology, University of Twente, P. O. Box 217, 7500 AE Enschede, The Netherlands
[b] Physikalisches Institut and Center for Nanotechnology (CeNTech) Westfälische Wilhelms-Universität Münster, Heisenbergstraße11, D-48149 Münster, Germany
[c] Condensed Matter and Interfaces, Debye Institute, University of Utrecht, P. O. Box 80.000, 3508 TA Utrecht, The Netherlands
[d] Current address: Université de Strasbourg – Institut de Science et d'Ingénierie Supramoléculaires (ISIS), 8 Alleé Gaspard Monge, 67083 Strasbourg, France
S. Ramachandra and C. A. Strassert have equally contributed to the paper.

Reprint requests to Prof. Luisa De Cola. E-mail: decola@unistra.fr

Z. Naturforsch. **2014**, *69b*, 263 – 274 / DOI: 10.5560/ZNB.2014-3323
Received December 11, 2013

This work describes the synthesis and photophysical characterization of Ir(III) and Ru(II) complexes bearing terminal amino groups, which act as anchoring units for the attachment to quantum dots, QDs. The photophysical properties of the metal complexes in combination with different types of QDs, allows directional photoinduced processes in the assemblies. In particular, we show photoinduced energy transfer from the luminescent excited Ir(III) unit to the CdTe nanocrystals, with an efficiency of 40 %. The directionality was then inverted by employing an emitting Ru(II) complex as energy acceptor, in combination with photoluminescent CdSe/ZnS quantum dots. The efficiency of the photoinduced energy transfer from the nanocrystals to the Ru(II) center was estimated to be as high as 75 %. This work provides model systems for nanoassemblies based on quantum dots and metal complexes for optoelectronic applications, and as active light-harvesting systems.

Key words: Luminescent Metal Complexes, Quantum Dots, Nanoassemblies, Photoinduced Energy Transfer

Introduction

Quantum dots (QDs) have been in the limelight for the past three decades due to their fascinating size-dependent optical and electrical behavior, owing to the quantum confinement of charge carriers [1 – 8]. This allows the fabrication of semiconducting materials with different band gaps by just varying their sizes, which is not possible in bulk semiconductors [9]. In addition to the size tunability, these nanomaterials also exhibit a very narrow emission profile and high photostability, which makes them a viable alternative to fluorescent organic molecules for numerous applications like imaging *in vitro* and *in vivo* [10 – 13], sensors [14, 15], lasers [16, 17], and optoelectronic devices [18 – 25]. These nanocrystals are obtained by solvothermal methods, yielding various sizes of QDs with a high degree of monodispersity [26]. Conventionally, these materials are synthesized in a coordinating solvent like trioctylphosphine (TOP) or trioctylphosphine oxide (TOPO). In addition, they are also capped with ligands like dodecylamine (DDA), hexadecylamine (HDA) or oleic acid (OA). In most cases, the capping agent is only a solubilizing and protecting group without any specific photo- or electroactive functionality. On the other hand, recent reports on the exchange of the TOP and TOPO ligands with chromophores such as metal complexes of Ru(II) [27 – 32], Ir(III) [11] and Os(II) [33] bearing amino, thiol or carboxylic functionalities were described in the literature. A clever design of the anchoring molecules can lead to the promotion of charge or energy transfer from or

to the nanocrystals. These processes can be directionally controlled by combining the appropriate QDs with electron acceptor or donator moieties. Such combinations could lead to assemblies in which all the energy is funneled into a single component (light harvesting), or where the charges are accumulated in a moiety and eventually used for chemical transformations.

In order to exploit such processes, we have chosen two metal complexes based on Ir(III) and Ru(II). Both complexes possess terminal amino groups to anchor them to the surface of the QDs. Due to their very different electrochemical and photophysical properties, they can act as energy donor or acceptor units, respectively, in combination with QDs. The rationale behind using these metal complexes is that they are not only photoluminescent, but can also emit light by charge injection and recombination. The possibility to use electrically generated excited states could then be exploited to sensitize QDs in devices, as for instance organic light emitting diodes (OLEDs) [34 – 37]. In order to study the photoinduced processes of the metal complexes anchored on the surfaces of quantum dots, we have chosen red-emitting CdTe QDs coated with TOP and DDA in combination with the yellow-orange-emitting Ir(III) complex. Due to the difference in energy of the excited states we expect a photoinduced energy transfer from the excited metal complex to the nanocrystals.

For inverting the directionality of the process, we have selected a Ru(II) complex, which emits in the red region, and has been derivatized at one of the ligands with a terminal amino group that allows the coordination (*via* carbon disulfide, CS_2, through a dithiocarbamate linkage) to the surface of blue emitting ZnS-capped CdSe QDs. The assembly utilizes the high absorption cross section of QDs, acting as a light-harvesting system, and funnels the energy to the lower energy state of the luminescent metal complex. Such an array involving an antenna mechanism can serve as a model system for light harvesting in a photoactive center for solar energy conversion [19, 38 – 40]. The reason to change the metal ion and shift from Ir(III) to Ru(II) complexes for switching the energy transfer direction relies on the fact that we believe that the most efficient mechanism for these assemblies is Förster energy transfer. Therefore, a good spectral overlap between the emission of the donor and the absorption of the acceptor is required. Such condition cannot be fulfilled using the same Ir(III) complex employed for QD sensitization, since it does not absorb at wavelengths above 420 – 450 nm, where the emission of the available blue emitting QDs occurs.

In this paper, we report the syntheses of two tailored luminescent metal complexes, namely 4{4-[4-(4-aminophenyl)-phenyl]-2,2′-bipyridine-$\kappa N^1,\kappa N^{1'}$}-bis-(2-phenylpyridine-$\kappa N^1,\kappa C^{2'}$)iridium(III) hexafluorophosphate (**3**) and {4-[4-(4-aminophenyl)-phenyl]-2,2′-bipyridine-$\kappa N^1,\kappa N^{1'}$}-bis-(2,2′-bipyridine-$\kappa N^1,\kappa N^{1'}$)ruthenium(II) bis-hexafluorophosphate (**6**). The complexes have been fully characterized and their photophysical properties investigated. Nanoassemblies involving these metal complexes and QDs are also reported, and photoinduced electronic energy transfer processes have been quantitatively investigated. The results show that efficient processes can be achieved with both types of assemblies.

Results and Discussion

Synthesis and photophysical characterization of the metal complexes

*Synthesis of **3***

The synthesis of neutral and charged Ir(III) complexes have received a lot of attention over the years [41 – 43]. Our synthetic procedure is shown in Scheme 1. 4-(4-aminophenyl)-phenyl-2,2′-bypridine (**2**) was reacted with the dichloro-bridged iridium(III) complex **1** following a procedure reported by Plummer *et al.* [44], yielding **3**, a dicationic heteroleptic compound with two phenyl units between the Ir(III) core and the terminal amino group.

*Synthesis of **6***

Several strategies have been reported for the synthesis of Ru(II) polypyridyl complexes [45 – 51]. However, the common synthetic route based on the preparation of the bis-(2,2′-bipyridine-$\kappa N^1,\kappa N^{1'}$)-bis-chloridoruthenium(II) precursor and subsequent reaction with 4-(4-aminophenyl)-phenyl-2,2′-bypridine (**2**) resulted in very poor yields of the desired product. Therefore, a three steps synthesis was performed (Scheme 2), as reported by Welter *et al.* [51], complexing bis-(2,2′-bipyridine-$\kappa N^1,\kappa N^{1'}$)-bis-chloridoruthenium(II) with 4-(4-bromophenyl)-2,2′-bypridine in ethylene glycol under microwave irradiation (450 W) which resulted in the dicationic

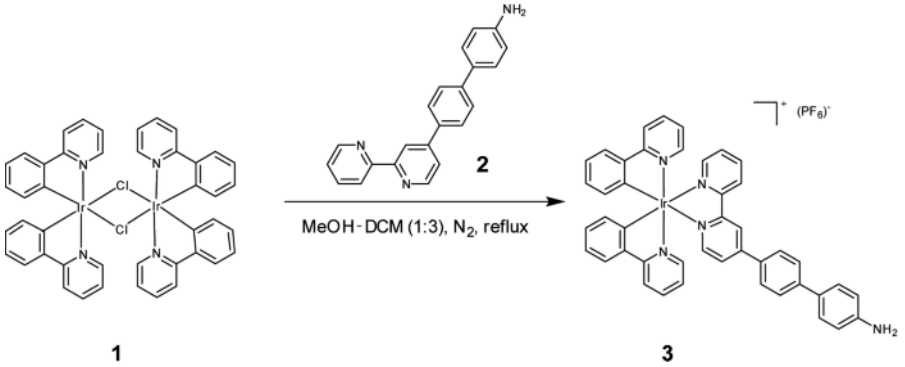

Scheme 1. Schematic route for the synthesis of {4-[4-(4-aminophenyl)-phenyl]-2,2′-bipyridine-$\kappa N^1,\kappa N^{1'}$}-bis-(2-phenylpyridine-$\kappa N^1,\kappa C^{2'}$)iridium(III) hexafluorophosphate (**3**).

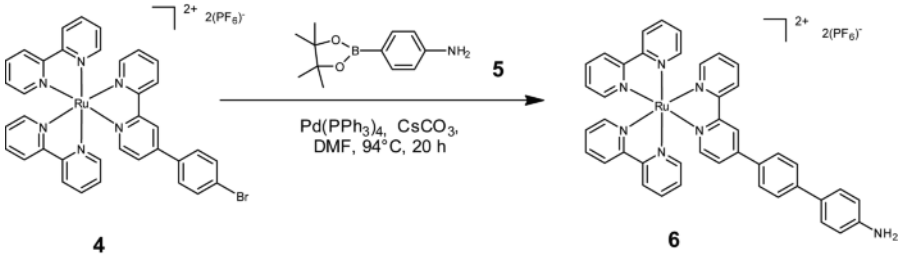

Scheme 2. Synthesis of {4-[4-(4-aminophenyl)-phenyl]-2,2′-bipyridine-$\kappa N^1,\kappa N^{1'}$}-bis-(2,2′-bipyridine-$\kappa N^1,\kappa N^{1'}$)ruthenium(II) bis-hexafluorophosphate (**6**).

complex **4**. Then, a Pd(0)-catalyzed cross-coupling reaction with **5** gave the final product **6** in good yields (about 85 %).

*Comparative photophysics of **3** and (2,2′-bipyridine-$\kappa N^1,\kappa N^{1'}$)-bis-(2-phenylpyridine-$\kappa N^1,\kappa C^{2'}$)-iridium(III) hexafluorophosphate (**3′**)*

The photophysical characterization of **3** is reported here in comparison to a reference complex, (2,2′-bipyridine-$\kappa N^1,\kappa N^{1'}$)-bis-(2-phenylpyridine-$\kappa N^1,\kappa C^{2'}$)iridium(III) hexafluorophosphate (**3′**). The photophysical data are summarized in Table 1. Fig. 1 shows the steady state absorption spectra of **3** and **3′** in CH_3CN solutions. Both exhibit similar absorption profiles around 250 nm, with absorption coefficients close to $3.7 \times 10^4\,L\,mol^{-1}\,cm^{-1}$. This band is attributed to intraligand transitions (IL, $\pi \rightarrow \pi^*$ phenylpyridine and bipyridine ligands) [53]. The energetically lowest electronic transitions for **3′** (around 380 nm) correspond to the much weaker metal to ligand charge transfer processes ($d\pi \rightarrow \pi^*$, ^{1}MLCT), with a molar absorption coefficient of

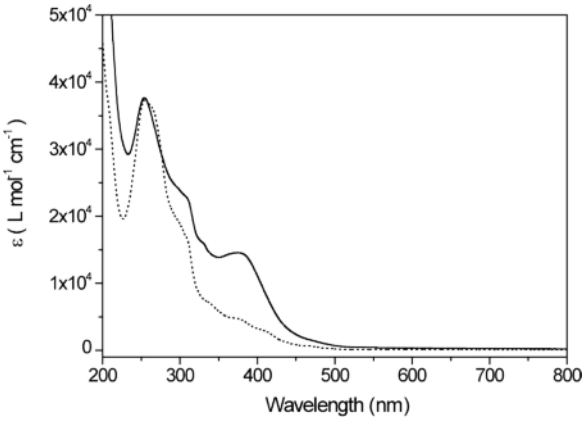

Fig. 1. Absorption spectra of **3** (–) and **3′** (···) in CH_3CN.

the order of $10^3\,L\,mol^{-1}\,cm^{-1}$. They involve the *d* orbitals of the metal atom and the π^* orbitals of the bipyridine ligand. The lowest energy absorptions are due to transitions from the singlet ground state to the ^{3}MLCT excited states, which for iridium(III) and other heavy atoms are partially allowed due to strong spin orbit coupling [53 – 55] and can be observed between

Table 1. Photophysical properties of **3**, (2,2′-bipyridine-$\kappa N^1,\kappa N^{1'}$)-bis-(2-phenylpyridine-$\kappa N^1,\kappa C^{2'}$)iridium(III) hexafluorophosphate (**3′**), **6**, and tris-(2,2′-bipyridine-$\kappa N^1,\kappa N^{1'}$)ruthenium(II) bis-hexafluorophosphate (**6′**).

System	Emission, 298 K[a]							Emission, 77 K[b]	
	λ_{max} (nm)	Φ aerated[c]	τ (ns) aerated	Φ deaerated[c]	τ (μs) deaerated	k_r (10^5 s^{-1})	k_{nr} (10^5 s^{-1})	λ_{max} (nm)	τ (μs)
3	585[d]	0.001	326	0.020	1.4	0.14	7.0	553[d]	83.8
3′	602[d]	0.008	355	0.075	1.2	0.63	7.7	532[d]	5.4
6	620[e]	0.009	155	0.023	1.2	0.19	8.1	588[e]	6.4
6′	611[f]	0.016[f]	117	0.059[f]	0.9[f]	0.66[f]	10.6[f]	579[e]	5.7

[a] All data for complexes in CH_3CN, except otherwise specified; [b] in butyronitrile glassy matrix; [c] quantum yields (Φ) were measured against aerated tris-(2,2′-bipyridine-$\kappa N^1,\kappa N^{1'}$)ruthenium(II) bis-hexafluorophosphate in CH_3CN ($\Phi = 0.016$); [d] $\lambda_{ex} = 350$ nm; [e] $\lambda_{ex} = 450$ nm; [f] obtained from ref. [52].

380 and 450 nm. However, in the case of **3**, a much stronger band ($\varepsilon = 14\,500\,\mathrm{L\,mol^{-1}\,cm^{-1}}$) around 380 nm is observed. The origin of this absorption feature is attributed to π–π^* transitions involving the two conjugated phenyl rings which strongly couple with the pyridine ring [55]. This stronger band masks the less intense one related to the ^{1}MLCT transitions. Both complexes exhibit orange luminescence, centered for **3** at 585 nm and for **3′** at 602 nm.

The emission profile is broad and structureless with a large Stokes shift, as shown in Fig. 2, which is typical for luminescence from a ^{3}MLCT state. Compared to **3′**, the emission of **3** is blue shifted by 17 nm (483 cm^{-1}). This can be explained by the electron donating effect of the amino group, which increases the energy of the LUMO of the substituted bipyridine ligand. Consequently, since the lowest MLCT states involve indeed the LUMO of the bipyridine, the HOMO-LUMO gap increases and results in a blue shifted emission. The effect exerted by the amino group is predominant, despite the presence of two phenyl rings, which should cause a red shift by extending the conjugation. This is evident from the fact that the emission maximum of **3** lies between that of **3′** (602 nm) and [4-(4-aminophenyl)-2,2′-bipyridine-$\kappa N^1,\kappa N^{1'}$]-bis-(2-phenylpyridine-$\kappa N^1,\kappa C^{2'}$)iridium(III) hexafluorophosphate (553 nm) [56]. The low temperature emission spectrum of **3** at 77 K in butyronitrile matrix (Fig. 2) shows a maximum at 553 nm. Such blue shift is typical for luminescent states possessing CT character and a higher polarity of the excited state compared with the ground state. The frozen solvent cannot stabilize the more polar excited state as efficiently as in fluid solution; therefore a destabilization of the excited state occurs.

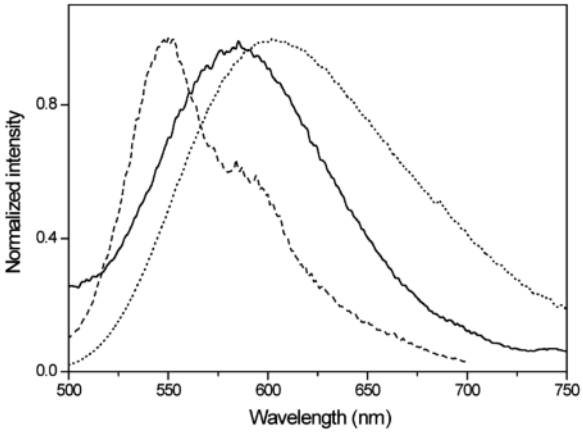

Fig. 2. Emission spectra of **3** (–) and **3′** (···) in CH_3CN. Emission spectrum of **3** measured at 77 K (- - -) in butyronitrile matrix ($\lambda_{ex} = 375$ nm).

*Comparative photophysics of **6** and tris-(2,2′-bipyridine-$\kappa N^1,\kappa N^{1'}$)ruthenium(II) bis-hexafluorophosphate (**6′**)*

The photophysical properties of **6** and *tris*-(2,2′-bipyridine-$\kappa N^1,\kappa N^{1'}$)ruthenium(II) bis-hexafluorophosphate (**6′**) are listed in Table 1. The steady state absorption spectra of **6** and **6′** are presented in Fig. 3. The intense absorption bands around 290 nm for both complexes are attributed to intraligand electronic transitions involving the bipyridine ligands (IL, $\pi \rightarrow \pi^*$) [57, 58]. Both complexes possess a low-energy transition around 450 nm, which is assigned to metal to ligand charge transfer (^{1}MLCT, $d\pi \rightarrow \pi^*$). The less intense bands around 240 nm are attributed to higher MLCT transitions for both complexes. In the case of **6′**, the weak bands around 344 nm are assigned to the metal-centered (MC) transitions [57, 58].

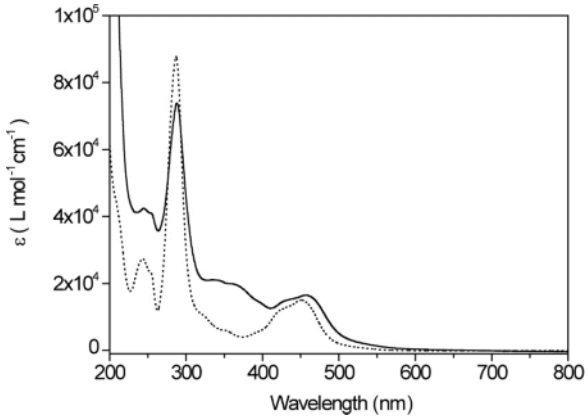

Fig. 3. Absorption spectra of **6** (–) and **6′** (···) in CH_3CN.

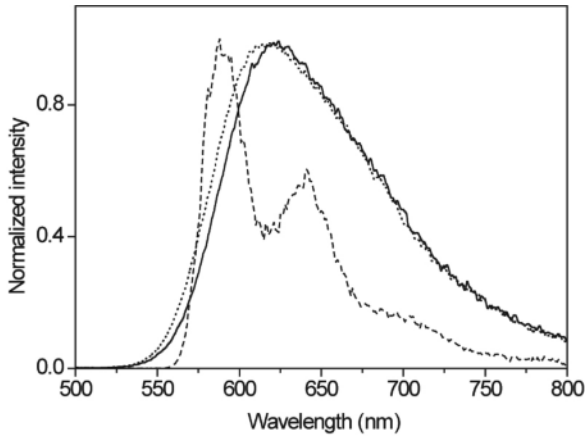

Fig. 4. Emission spectra of **6** (–) and **6′** (···) in CH_3CN. Emission spectrum of **6** at 77 K (- - -) in butyronitrile matrix ($\lambda_{ex} = 450$ nm).

However, in the case of **6**, these bands are masked by the more pronounced absorptions which originate from the transitions involving the two phenyl rings.

Exciting these complexes in the visible region in a CH_3CN solution results in a broad emission profile, that is characteristic of complexes with an emissive ^{3}MLCT state. The emission maximum for **6** is centered at 620 nm, and for **6′** at 611 nm (Fig. 4). The minor red shift in the emission spectrum of **6** is most likely due to the enhanced conjugation [51] of the involved substituted bipyridine ligand, which is largely compensated by the electron donation exerted by the terminal amino group (*vide supra*). At 77 K, **6** has a structured emission profile that appears blue shifted by about 30 nm with respect to the r. t. emission, a consequence of the solvatochromism of ^{3}MLCT states [57, 58]. The clear vibrational progression observed in glassy matrices points to a partial mixing with a ^{3}LC state, which is also reflected by the smaller radiative rate constant of **6** (see Table 1).

Photophysical characterization of the nanoassemblies

*CdTe-**3** nanoassembly*

The choice of red-emitting CdTe in combination with **3** stems from the excellent spectral overlap between the emission of the metal complex and the absorption profile of the QDs (see Fig. S1; Supporting Information available online. See note at the end of the paper for availability). Fig. 5 shows the absorption spectra of CdTe-**3** nanoassemblies, and of the individual components. The absorption profile of the assembly equals the sum of both constituents. The emission spectra of CdTe, **3** and CdTe-**3** are shown in Fig. 6 (left panel), and were acquired by exciting the samples at 385 nm, which corresponds to the absorption maximum of **3**. Since QDs absorb at all wavelengths shorter than their exciton absorption, it is not possible to selectively excite the donor in the presence of the nanocrystals. However the absorption spectra (Fig. 5) clearly show that the absorption of the assembly is the sum of the two components. The emission spectrum of the assembly has contributions from both **3** as well as CdTe, since both absorb at the excitation wavelenght of 385 nm. The spectra suggest that there is a quenching of the Ir(III) component and a sensitization of the QD

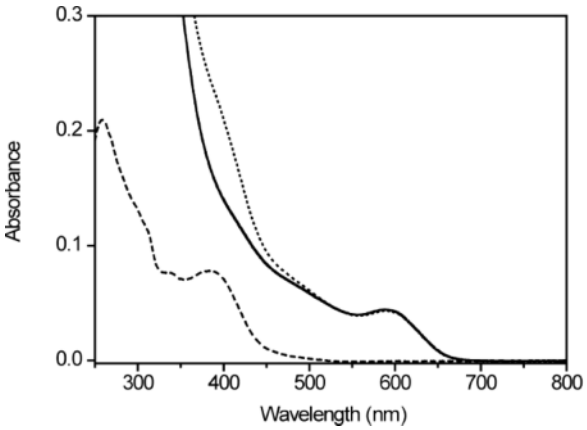

Fig. 5. Absorption spectra of CdTe (–), **3** (- - -) and CdTe-**3** (···) in DCM.

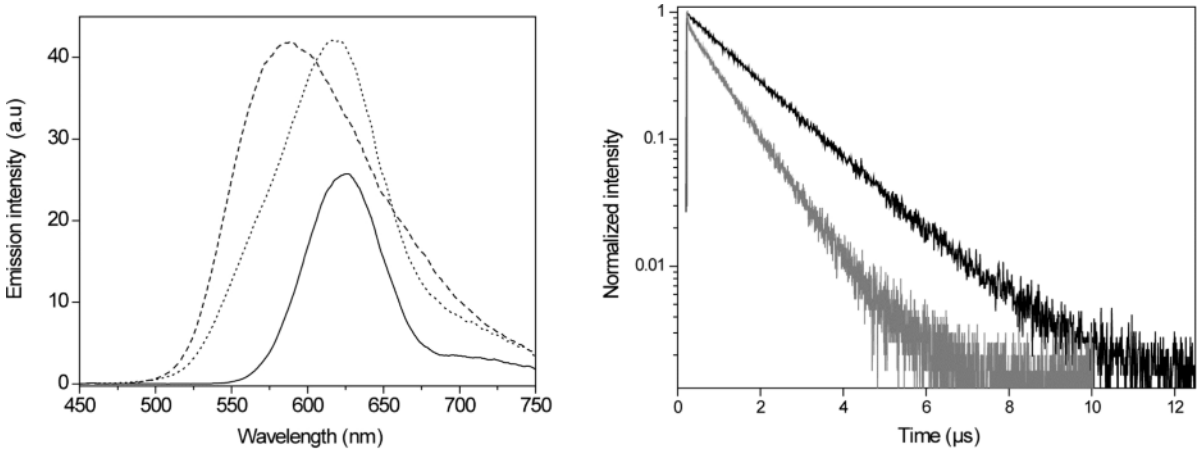

Fig. 6. Left panel: Emission spectra of CdTe (–), **3** (- - -) and CdTe-**3** (···) in DCM ($\lambda_{ex} = 385$ nm). Right panel: Quenched lifetime of **3** in the assembly (grey decay curve), as compared to **3** in absence of any acceptor (black decay curve).

emission. Such a result can be interpreted as a photoinduced energy transfer from the excited Ir(III) complex to the QD. In order to estimate the efficiency of this process, the emission spectrum of the assembly can be expressed as a linear combination of the individual constituents (see Fig. S2). This analysis facilitates the quantification of the donor quenching and the sensitization of the acceptor by energy transfer (*vide infra*).

The lifetime of **3** in the absence of the acceptor is 1.4 μs, which in the presence of the nanocrystals is quenched to a mono-exponential decay of 849 ns. On the other hand, the pre-exponential factor- weighted average lifetime of the tri-exponential decay from CdTe (9 ns) did not vary significantly upon binding of **3**. These findings support our argument of photoinduced energy transfer from the bound Ir(III) complexes to the QDs. As a control experiment, **3′**, which lacks any anchoring group, was investigated in combination with CdTe nanocrystals under identical experimental conditions. The emission of the mixture was separated into the individual constituents, and a 30 % quenching of the metal complex was observed, with no concomitant sensitization of the QDs (see Fig. S3). However, no significant shortening of the excited state lifetime of CdTe or **3′** was observed, which possibly suggests static quenching processes.

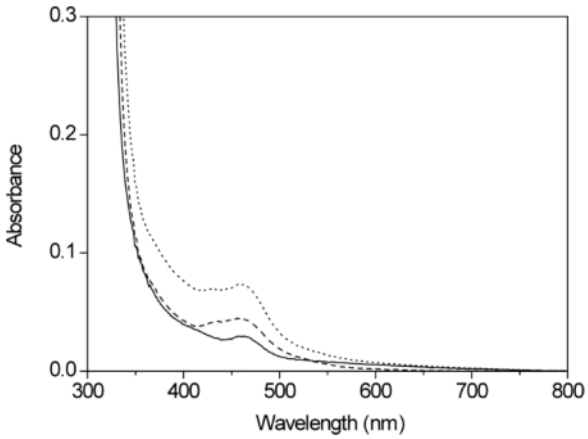

Fig. 7. Absorption spectra of CdSe/ZnS (–), **6** (- - -) and CdSe/ZnS-**6** (···) in 1 : 1 (v/v) MeOH-toluene.

*CdSe/ZnS-**6** nanoassembly*

In order to demonstrate the energy transfer in the opposite direction, we chose CdSe/ZnS as the donor and **6** as the energy acceptor, dictated by a good spectral overlap (see Fig. S4). Due to the presence of the ZnS shell, we employed a different strategy to enhance the binding of **6** to the nanocrystals' surface. We used the procedure reported by Dubois *et al.* [59], who describe the coordination of amines to the surface of CdSe/ZnS with the aid of CS_2 through a dithiocarbamate complex.

The absorption spectra of CdSe/ZnS-**6** and its individual components are depicted in Fig. 7. The absorption profile of the assembly equals the sum of both constituents. The excitation wavelength for the steady state emission was fixed at 430 nm.

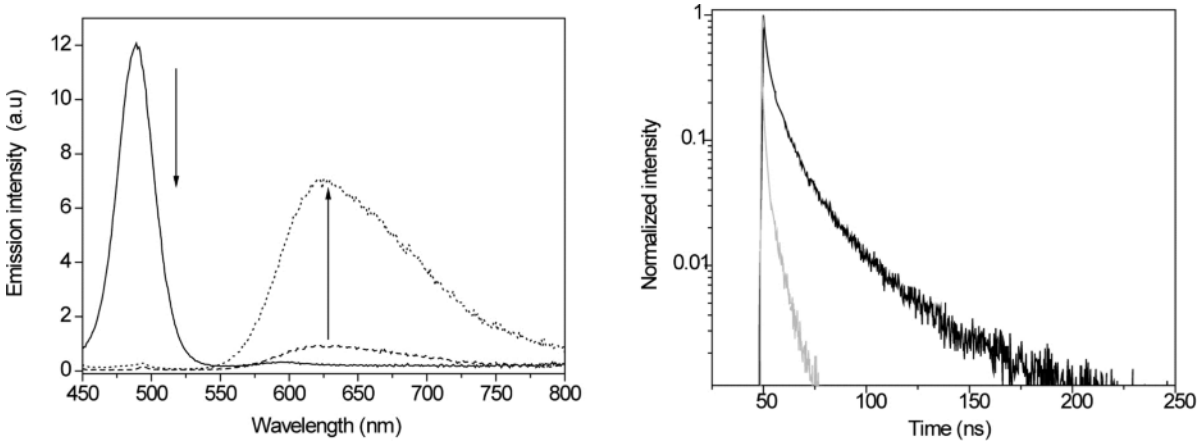

Fig. 8. Left panel: Emission spectra of CdSe/ZnS (–), **6** (- - -) and CdSe/ZnS-**6** (···) in 1 : 1 (*v*/*v*) MeOH-toluene. Right panel: Quenching of QD lifetimes in the assembly (grey decay curve) as compared to the QDs in absence of any acceptor (black decay curve).

Since QDs absorb at all wavelengths below their exciton absorption, it is not possible to selectively excite the donor in the presence of the nanocrystals. It is evident by comparison of the assembly and its individual components (left panel, Fig. 8), that the QD emission is almost completely quenched, and the emission of the Ru(II) complex is significantly sensitized. This is also mirrored in the lifetime reduction of the nanocrystals (right panel, Fig. 8). The average lifetime of CdSe/ZnS was calculated by weighing each component by its pre-exponential factor, and was shortened from 20.9 to 5.7 ns within the assembly. On the other hand, the lifetime of **6** (1.2 μs) did not vary significantly upon binding to CdSe/ZnS. These findings support our argument of a photoinduced energy transfer from the QDs to the bound Ru(II) complexes. A control experiment with **6′** showed a 20 % quenching of the QD emission, but no sensitization of the Ru(II) complex (see Fig. S5). In addition, no significant lifetime changes were observed, which possibly suggests static quenching processes. An analogous behavior was observed when the experiment was carried out in the absence of CS_2. The energy transfer from the nanocrystal to the Ru(II) complex is therefore unambiguously enabled by the binding interaction.

Energy transfer analysis

The energy transfer efficiency, E, can be expressed alternatively in terms of the lifetimes or the emission intensities of the donor, in the absence or presence of the acceptor, according to Eq. 1 [60],

$$E = 1 - \frac{\tau}{\tau_0} = 1 - \frac{F}{F_0} \tag{1}$$

where τ and F, τ_0 and F_0 denote the lifetimes and the areas under the emission spectra of the donor, in the presence or absence of the acceptor, respectively. Energy transfer can also be quantified by the extent of sensitization of the acceptor, according to Eq. 2,

$$E = \frac{(1 - 10^{-Aa})}{(1 - 10^{-Ad})} \left[\frac{F_{AD}}{F_A} - 1 \right] \tag{2}$$

where $(1-10^{-Aa})$ and $(1–10^{-Ad})$ are the fractions of light absorbed by the acceptor and the donor, respectively, at the excitation wavelength of the donor, and F_{AD} and F_A are the areas under the emission spectra of the acceptor, in presence and absence of the donor, respectively.

Table 2. FRET parameters for the nanoassemblies.

Assembly	J ($cm^6\ mol^{-1}$)	E	R_0 (Å)	r (Å)	k_{ET} (s^{-1})
CdTe-**3**	7.05×10^{-10}	0.40	35.5	37	5×10^5
CdSe/ZnS-**6**	4.38×10^{-11}	0.75	36.4	34	1×10^8

*CdTe-**3** nanoassembly*

In the CdTe-**3** assembly, it is not possible to selectively excite the donor complex. However, the concentrations of CdTe and **3** within the assemblies (0.5 μM :

5 μM) were kept identical to a set of two reference solutions (CdTe: 0.5 μM, **3**: 5 μM). Therefore, the fraction of light absorbed by each component is the same within the assembly and the corresponding reference solution. On the other hand, the emission spectrum of the CdTe-**3** assembly has contributions from both **3** and CdTe, but can be expressed as a linear combination of the spectra of the individual constituents (see Fig. S2). Consequently, the area under the emission curve of each component within the assembly can be easily calculated and compared with the corresponding emission spectra of the reference solutions.

The energy transfer efficiency was calculated to be 40 % by considering the lifetimes of **3** in the presence and absence of CdTe (Eq. 1). The sensitization of CdTe by **3** was calculated to be 42.5 % (Eq. 2). Both results are in good agreement within the experimental error. However, the luminescence of **3** is quenched by 65 % within the assembly, which can be rationalized considering that for the control experiment with **3′**, which lacks any anchoring group, a 30 % quenching of the emission was observed, without significant decrease in the excited state lifetime.

*CdSe/ZnS-**6** nanoassembly*

In this case, it is also not possible to selectively excite the donor. However, the concentrations of CdSe/ZnS and **6** within the assemblies (1 μM : 10 μM) were kept identical to a set of two reference solutions (CdSe/ZnS: 1 μM; **6**: 10 μM). Therefore, the fraction of light absorbed by each component is the same within the assembly and the corresponding reference solution. In this case, the emission spectra of both CdSe/ZnS and **6** are clearly resolved. Consequently, the area under the emission curve of each component can be easily calculated and compared with the corresponding emission spectra from the reference solutions. CdSe/ZnS exhibited tri-exponential decays, both in the presence and absence of the acceptor. In order to estimate the energy transfer efficiency, the average lifetime of CdSe/ZnS was calculated by weighing each component by its pre-exponential factor. Within this approximation, the energy transfer efficiency can be estimated as 73 % (Eq. 1). The luminescence of CdSe/ZnS is quenched by 95 % within the assembly, which can be rationalized by considering the control experiment with **6′**, which lacks any anchoring group. In this case, a 20 % quenching of the CdSe/ZnS emission was observed. An attempt to quantify the extent of sensitization (Eq. 2) of **6** by CdSe/ZnS led to efficiencies above 100 %, which points to an effective sensitization and to an enhanced brightness of the metal complex. Similar findings were reported by Bawendi *et al.* [33] in assemblies of CdZnSe/CdZnS QDs and Os(II) complexes, where the QDs sensitized the emission of the metal center.

Orbital overlap between the donor and acceptor constitutes the main prerequisite for energy transfer by electron exchange. Therefore, the energy transfer rate by the Dexter-type mechanism decreases exponentially with the distance [61] approaching negligibly small values beyond 10 Å. In the case of **6** and CdSe/ZnS QDs, the photoactive core is capped by a ZnS shell that hinders the electron exchange between the donor and the acceptor. From the absorption spectrum of the CdTe-**3** assembly it was evident that the donor and acceptor do not interact in the ground state, which points to a poor orbital overlap.

There is a good spectral overlap for both CdTe-**3** and CdSe/ZnS-**6** nanoassemblies, and the radiative rate constant of the CdSe/ZnS donor is of the order of $10^7\ s^{-1}$, and of $10^5\ s^{-1}$ for the Ir(III) complex. The molar absorption coefficient of the Ru(II) complex acceptor is of the order of $10^4\ L\ mol^{-1}\ cm^{-1}$, whereas for the CdTe QD it is around $10^5\ L\ mol^{-1}\ cm^{-1}$. The photoinduced energy transfer by the Förster mechanism is therefore favored [62 – 64]. It is possible to estimate the Förster resonance energy transfer (FRET) parameters for the nanoassemblies. The energy transfer rate constant, k_{ET}, is given by the Eq. 3,

$$k_{ET} = \frac{\Phi_D \kappa^2}{\tau_D r^6}\left(\frac{9000(\ln 10)}{128\pi^5 N n^4}\right)\int_0^\infty F_D(\lambda)\varepsilon_A\,(\lambda)\lambda^4 d\lambda \tag{3}$$

where Φ_D is the quantum yield of the donor, κ^2 is the orientation factor which depends on the angle between the electronic transition dipole moments, τ_D is the lifetime of the donor in absence of the acceptor, r is the donor-acceptor separation, and n is the refractive index of the environment. $F_D(\lambda)$ is the corrected fluorescence intensity of the donor at a given wavelength λ, with maximum intensity normalized to unity. $\varepsilon_A(\lambda)$ is the molar absorption coefficient of the acceptor at a given wavelength λ. The integral of Eq. 1 is commonly referred to as the spectral overlap integral, J. κ^2 was assumed to be $2/3$; the quantum yield of CdSe/ZnS was provided by the supplier as 0.4. Eq. 3 can be rewritten

as follows (Eq. 4),

$$k_{ET} = \frac{1}{\tau_D}\left(\frac{R_0}{r}\right)^6 \quad (4)$$

where R_0 is the Förster radius. The energy transfer efficiency, E, can be expressed in terms of R_0 and the donor-acceptor separation, r (Eq. 5):

$$E = \frac{R_0^6}{R_0^6 + r^6} \quad (5)$$

Therefore, the dependence of E on r/R_0 can be plotted as a sigmoidal curve (see Fig. S6). Since the energy transfer efficiency is known (*vide supra*), and R_0 can be calculated from experimental parameters as described above, it is possible to compute the effective donor-acceptor separation, r. The resulting FRET parameters (J, E, R_0, r and k_{ET}) for both assemblies are summarized in Table 2. The energy transfer rate constants calculated according to Eq. 4 are in excellent agreement with the ones obtained from the lifetimes of the donor species, in the presence and absence of the acceptors, according to Eq. 6:

$$k_{ET} = \frac{1}{\tau} - \frac{1}{\tau_0} \quad (6)$$

k_{ET} for CdTe-**3** is $4.6 \times 10^5\ s^{-1}$, and for CdSe/ZnS-**6** is $1{,}3 \times 10^8\ s^{-1}$. Furthermore, the computed effective donor-acceptor separations ($\sim$ 35 Å) are reasonable considering the biphenyl-amino spacer between the metal complex and the nanocrystals.

Conclusions

Our model systems allowed us to demonstrate the feasibility of bidirectional energy transfer between metal complexes and QDs in solution-processed nanoassemblies. The possibility of transferring the excitation energy from electroluminescent metal complexes to QDs acting as acceptors opens up the possibility to drive the nanocrystals electrically, which is a limiting factor for the application of these nanomaterials for light generation. On the other hand, sensitizing a Ru(II) complex with QDs serves as a model system for light-harvesting applications. Such assemblies take advantage of the excellent absorption cross section of the nanocrystals and funnel the excitation energy to the Ru(II) complexes attached to their surface.

Experimental Section

Chemicals

All the chemicals were bought from Sigma-Aldrich and used without further purification, unless specified. (2,2′-Bipyridine-$\kappa N^1,\kappa N^{1'}$)-bis-(2-phenylpyridine-κN^1, $\kappa C^{2'}$)iridium(III) hexafluorophosphate (**3′**) was synthesized according to a literature procedure [65], whereas tris-(2,2′-bipyridine-$\kappa N^1,\kappa N^{1'}$)ruthenium(II) bis-hexafluorophosphate (**6′**) was purchased from Sigma-Aldrich and was used without further purification. Bis-(2,2′-bipyridine-$\kappa N^1,\kappa N^{1'}$)ruthenium(II) dichloride was synthesized according to a literature procedure [50].

*Synthesis of 4-[4-(4-aminophenyl)-phenyl]-2,2′-bypridine (**2**)*

4-(4-Bromophenyl)-2,2′-bypridine, was synthesized according to a literature procedure [51]. 0.502 g of 4-(4-bromophenyl)-2,2′-bypridine (1.6 mmol), 0.388 g of 4-aminophenyl-boronic acid pinacolester (**5**) (1.8 mmol), 0.092 g of $Pd(PPh_3)_4$ (0.08 mmol), and 0.577 g of Cs_2CO_3 (1.8 mmol) were reacted at 100 °C in DMF under N_2 overnight. After cooling to r. t., the mixture was separated between water and DCM. The organic phase was dried over $MgSO_4$, and the solvent was removed under reduced pressure to yield 0.717 g of a brown precipitate. Flash column chromatography with a polarity gradient was used to purify the compound. Hexane : ethyl acetate : triethylamine mixtures were used with the following ratios. 8 : 2 : 1 (300 mL), 5 : 2 : 1 (320 mL) and 4 : 4 : 1 (100 mL). The fractions with the product were combined and the solvents were removed under reduced pressure to give a dark-yellow solid, which was dissolved in DCM and washed with a 2 M NaOH solution in water. The organic phase was dried, and the solvent removed to yield a bright-yellow compound. Yield: 270 mg (52 %). – ^{1}H NMR ($CDCl_3$, 300 MHz): δ(ppm) = 8.76 – 8.74 (d, 3 H), 8.54 – 8.52 (d, J = 7.8 Hz, 2 H), 7.91 – 7.83 (m, 3 H), 7.70 – 7.67 (d, J = 8.4 Hz, 2 H), 7.64 – 7.62 (m, 1 H), 7.51 – 7.48 (d, J = 8.4 Hz, 2 H), 7.39 – 7.35 (m, 1 H), 6.81 – 6.78 (d, J = 8.4 Hz, 2 H, -NH2). – EI-MS: m/z = 324.15 (100 %), expected: 323.14.

*Synthesis of {4-[4-(4-aminophenyl)-phenyl]-2,2′-bipyridine-$\kappa N^1,\kappa N^{1'}$}-bis-(2-phenylpyridine-$\kappa N^1,\kappa C^{2'}$)iridium(III) hexafluorophosphate (**3**)*

Tetrakis-(2-phenylpyridine-$\kappa N^1,\kappa C^{2'}$)-bis-(chloro-μ)diiridium(III), (**1**) was synthesized according to a literature procedure [49]. 83 mg of **1** (0.522 mmol) and 44 mg of **2** (0.157 mmol) were dissolved in a round-bottom flask in

a solvent mixture of MeOH and DCM (1 : 3, 20 mL). The reaction mixture was refluxed for 3 h under N_2 atmosphere. The DCM was evaporated under reduced pressure. To the resulting solution an excess of methanolic NH_4PF_6 was added. The resulting yellow precipitate was filtered and washed with water and ether. The impure product was purified by column chromatography using silica gel and a mixture of 10 % NaCl solution in water, CH_3CN and MeOH (1 : 6 : 1). The resulting pure compound was an orange solid (105 mg). – ^{1}H NMR (400 MHz, CD_3CN): δ(ppm) = 8.77 (s, 2H), 8.08 (tt, 4H), 7.85 (m, J = 45.9 Hz, 10H), 7.67 (t, 2H), 7.51 (d, J = 8.3 Hz, 2H), 7.05 (t, 4H), 6.94 (t, 2H), 6.75 (d, J = 8.4 Hz, 2H), 6.31 (d, J = 7.4 Hz, 2H), 4.39 (s, broad, 2H). – HRMS (ESI): m/z = 824.23691 (100 %), expected: 824.23652.

*Synthesis of {4-[4-(4-aminophenyl)-phenyl]-2,2′-bipyridine-$\kappa N^1,\kappa N^{1'}$}-bis-(2,2′-bipyridine-$\kappa N^1,\kappa N^{1'}$)ruthenium(II) bis-hexafluorophosphate (**6**)*

[4-(4-Bromophenyl)-2,2′-bypridine-$\kappa N^1,\kappa N^{1'}$]-bis-(2,2′-bipyridine-$\kappa N^1,\kappa N^{1'}$)ruthenium(II) bis-hexafluorophosphate, (**4**) was synthesized according to a literature procedure [45 – 48, 51, 66 – 68]. In a Schlenk flask, 75 mg of **4** (0.0739 mmol), 80 mg of **5** (0.369 mmol) and 240 mg of Cs_2CO_3 (0.739 mmol) were taken in 10 mL of dry DMF. The flask was repeatedly degassed by freeze-pump-thaw technique (3 cycles). A catalytic amount of $Pd(PPh_3)_4$ was added under a steady flow of N_2, and the reaction mixture was heated at 94 °C for 20 h. The DMF was removed under vacuum, and toluene was added. The solid was washed with ether and purified by column chromatography (silica gel) using a mixture of 10 % NaCl solution in water, CH_3CN and MeOH as an eluent (300 mL water, 300 mL MeOH, 1200 mL CH_3CN, and 32 g NaCl). The organic solvents were removed, and the complex was precipitated by adding NH_4PF_6. The orange precipitate was filtered on celite, washed with water and then with ether. The pure complex was re-extracted using CH_3CN. The solvent was evaporated and finally dried at 50 °C over night under vacuum to yield 65 mg of pure complex. – ^{1}H NMR (300 MHz, CD_3CN): δ(ppm) = 8.79 (d, J = 1.2 Hz, 1H), 8.72 (d, J = 8.1 Hz, 1H), 8.55 (m, 4H), 8.11 (m, 5H), 7.93 (d, J = 8.4 Hz, 2H), 7.78 (m, 9H), 7.53 (d, J = 6.6 Hz, 2H), 7.42 (d, J = 5.1 Hz, 5H), 6.76 (d, J = 8.4 Hz, 2H), 4.42 (broad). – HRMS (ESI): m/z = 368.59187 (100 %), expected: 368.59258.

*Nanoassemblies of CdTe QDs and **3***

The synthesis of CdTe QDs of 5 nm diameter (λ_{em} = 620 nm) (CdTe) has been published elsewhere, [69]. 250 μL CdTe from the raw product (4.2×10^{-4} M) were dissolved in 400 μL of toluene. Concentrations of the QDs were determined by a literature procedure [70]. To this mixture was added 3 mL of MeOH to precipitate the nanocrystals, which were subsequently centrifuged. The supernatant was discarded, and the residue was dissolved in 10 mL of DCM and further diluted ten times to obtain a 10^{-6} M QD stock solution. Dispersions of the nanocrystals and solutions of Ir(III) complexes in DCM were prepared under inert atmosphere inside a glove box. 10^{-5} M stock solutions of Ir(III) complexes (**3** or **3′**) were prepared and mixed with the QDs dispersion, in such a way that the ratio of CdTe to Ir(III) complex was 1 : 10 and therefore their respective final concentrations 1 μM and 10 μM. The mixtures were allowed to stand for $\sim$ 1 h in order to ensure that the Ir(III) complex would displace a sufficient number of capping ligands from the QD surface.

*Nanoassemblies of CdSe/ZnS QD and **6***

ZnS-capped CdSe nanocrystals of 1.9 nm diameter (CdSe/ZnS) (λ_{em} = 490 nm) were provided by Evident Technologies, USA, as a dispersion in toluene. The QDs were washed using MeOH (following the same procedure as described above) in order to remove sufficient capping ligands, and redispersed in toluene. A 10 fold excess (relative to the nanocrystal concentration) of the Ru(II) complexes dissolved in MeOH was used for the ligand exchange. CdSe/ZnS (2 μM) and Ru(II) complexes (**6** or **6′**) (20 μM) in the presence of 555 μM CS_2 were employed. The same concentration of CS_2 was used with the reference solutions containing **6′**, in order to assure identical measuring conditions for comparative purposes. The resulting solutions were stirred at r. t. over night in order to form Ru(II) complex-functionalized quantum dots linked through dithiocarbamate complexation. All the samples in 1 : 1 (v/v) MeOH-toluene were degassed by bubbling N_2 for 40 min prior to the measurements.

Photophysics

Absorption spectra were measured on a Varian Cary 5000 double-beam UV/Vis NIR spectrometer and baseline corrected. Steady-state emission spectra were recorded on a Horiba Jobin-Yvon IBH FL-322 Fluorolog 3 spectrometer equipped with a 450 W xenon arc lamp, double grating excitation and emission monochromators (2.1 nm mm^{-1} dispersion; 1200 grooves mm^{-1}) and a TBX-4-X single-photon-counting detector. Emission spectra were corrected for source intensity (lamp and grating) and emission spectral response (detector and grating) by standard correction curves. Time-resolved measurements were performed using the time-correlated single-photon counting (TCSPC) option on the Fluorolog 3. NanoLED (402 nm; FWHM < 750 ps) with repetition rates between 10 kHz and 1 MHz were used to excite the samples. The excitation sources were mounted directly on the sample chamber at 90° to the emission beam.

The photons collected at the detector were correlated by a time-to-amplitude converter (TAC) to the excitation pulse. Signals were collected using an IBH DataStation Hub photon counting module, and data analysis was performed using the commercially available DAS6 software (Horiba Jobin Yvon IBH). The quality of fit was assessed by minimizing the reduced χ^2 function and visual inspection of the weighted residuals. All measurements were carried out in $10 \times 10\,mm^2$ quartz cuvettes, and spectroscopic grade solvents were employed.

Supporting information

Figs. S1–S6 are given as Supporting Information available online (DOI: 10.5560/ZNB.2013-3323).

Acknowledgement

NanoNed (project number AM7010) which is an initiative of the Dutch Ministry of Economic Affairs is acknowledged for financial support. The authors wish to thank Mr. Mathias Mydlak for providing compound **2**.

[1] A. P. Alivisatos, *J. Phys. Chem.* **1996**, *100*, 13226 – 13239.
[2] A. P. Alivisatos, *Science* **1996**, *271*, 933 – 937.
[3] V. I. Klimov in *Semiconductor and Metal Nanocrystals. Synthesis and Electronic and Optical Properties*, Marcel Dekker, New York **2004**.
[4] M. Nirmal, L. Brus, *Acc. Chem. Res.* **1999**, *32*, 407 – 414.
[5] A. L. Rogach (Ed.), *Semiconductor Nanocrystal Quantum Dots: Synthesis, Assembly, Spectroscopy and Applications*, Springer, Wien, New York, **2008**.
[6] V. I. Klimov (Ed.), *Nanocrystal Quantum Dots, Second Edition (Laser and Optical Science and Technology)*, CRC Press, Boca Raton, FL. **2010**.
[7] W. J. Parak, L. Manna, T. Nann, *Nanotechnology* **2008**, *1*, 73 – 96.
[8] Y. Masumoto, T. Takagahara (Eds.), *Semiconductor quantum dots. Physics, spectroscopy and applications*, Springer, Berlin, **2002**.
[9] C. B. Murray, C. R. Kagan, M. G. Bawendi, *Annu. Rev. Mater. Sci.* **2000**, 545 – 610.
[10] H. Daneshvar, J. Nelms, O. Muhammad, H. Jackson, J. Tkach, W. Davros, T. Peterson, M. A. Vogelbaum, M. P. Bruchez, S. A. Toms, *Nanomedicine* **2008**, *3*, 21 – 29.
[11] J.-M. Hsieh, M.-L. Ho, P.-W. Wu, P.-T. Chou, T.-T. Tsai, Y. Chi, *Chem. Commun.* **2006**, 615 – 617.
[12] Y. T. Lim, S. Kim, A. Nakayama, N. E. Stott, M. G. Bawendi, J. Frangioni, *Mol. Imaging* **2003**, *2*, 50 – 64.
[13] M. Bruchez, Jr., M. Moronne, P. Gin, S. Weiss, A. P. Alivisatos, *Science* **1998**, *281*, 2013 – 2016.
[14] J. Callan, A. De Silva, R. Mulrooney, B. Mc Caughan, *J. Inclusion Phenom. Macrocyclic Chem.* **2007**, *58*, 257 – 262.
[15] A. Y. Nazzal, L. Qu, X. Peng, M. Xiao, *Nano Lett.* **2003**, *3*, 819 – 822.
[16] V. I. Klimov, A. A. Mikhailovsky, S. Xu, A. Malko, J. A. Hollingsworth, C. A. Leatherdale, H. J. Eisler, M. G. Bawendi, *Science* **2000**, *290*, 314 – 317.
[17] C. Wang, B. L. Wehrenberg, C. Y. Woo, P. Guyot-Sionnest, *J. Phys. Chem. B* **2004**, *108*, 9027 – 9031.
[18] V. L. Colvin, M. C. Schlamp, A. P. Alivisatos, *Nature* **1994**, *370*, 354 – 357.
[19] I. Gur, N. A. Fromer, M. L. Geier, A. P. Alivisatos, *Science* **2005**, *310*, 462 – 465.
[20] P. V. Kamat, *J. Phys. Chem. C* **2008**, *112*, 18737 – 18753.
[21] A. Kongkanand, K. Tvrdy, K. Takechi, M. Kuno, P. V. Kamat, *J. Am. Chem. Soc.* **2008**, *130*, 4007 – 4015.
[22] K. S. Leschkies, R. Divakar, J. Basu, E. Enache-Pommer, J. E. Boercker, C. B. Carter, U. R. Kortshagen, D. J. Norris, E. S. Aydil, *Nano Lett.* **2007**, *7*, 1793 – 1798.
[23] T. Lopez-Luke, A. Wolcott, L. p. Xu, S. Chen, Z. Wen, J. Li, E. De La Rosa, J. Z. Zhang, *J. Phys. Chem. C* **2008**, *112*, 1282 – 1292.
[24] A. M. Munro, J. A. Bardecker, M. S. Liu, Y.-J. Cheng, Y.-H. Niu, I. J.-L. Plante, A. K. Y. Jen, D. S. Ginger, *Microchim. Acta* **2008**, *160*, 345 – 350.
[25] N. Tessler, V. Medvedev, M. Kazes, S. Kan, U. Banin, *Science* **2002**, *295*, 1506 – 1508.
[26] C. B. Murray, D. J. Norris, M. G. Bawendi, *J. Am. Chem. Soc.* **1993**, *115*, 8706 – 8715.
[27] W. Guo, J. Yuan, B. Li, Y. Du, E. Ying, E. Wang, *Analyst* **2008**, *133*, 1209 – 1213.
[28] P. A. S. Jorge, C. Maule, A. J. Silva, R. Benrashid, J. L. Santos, F. Farahi, *Anal. Chim. Acta* **2008**, *606*, 223 – 229.
[29] P. A. S. Jorge, M. Mayeh, R. Benrashid, P. Caldas, J. L. Santos, F. Farahi, *Appl. Opt.* **2006**, *45*, 3760 – 3767.
[30] I. L. Medintz, D. Farrell, K. Susumu, S. A. Trammell, J. R. Deschamps, F. M. Brunel, P. E. Dawson, H. Mattoussi, *Anal. Chem.* **2009**, *81*, 4831 – 4839.
[31] R. D. Schaller, M. Sykora, S. Jeong, V. I. Klimov, *J. Phys. Chem. B* **2006**, *110*, 25332 – 25338.
[32] M. Sykora, M. A. Petruska, J. Alstrum-Acevedo, I. Bezel, T. J. Meyer, V. I. Klimov, *J. Am. Chem. Soc.* **2006**, *128*, 9984.

[33] E. J. McLaurin, A. B. Greytak, M. G. Bawendi, D. G. Nocera, *J. Am. Chem. Soc.* **2009**, *131*, 12994 – 13001.
[34] P. O. Anikeeva, C. F. Madigan, S. A. Coe-Sullivan, J. S. Steckel, M. G. Bawendi, V. Bulovic, *Chem. Phys. Lett.* **2006**, *424*, 120 – 125.
[35] A. Rizzo, Y. Li, S. Kudera, F. Della Sala, M. Zanella, W. J. Parak, R. Cingolani, L. Manna, G. Gigli, *Appl. Phys. Lett.* **2007**, *90*, 051106 – 051103.
[36] J. M. Caruge, J. E. Halpert, V. Wood, V. Bulovic, M. G. Bawendi, *Nat. Photonics* **2008**, *2*, 247 – 250.
[37] S. Coe, W.-K. Woo, M. Bawendi, V. Bulovic, *Nature* **2002**, *420*, 800 – 803.
[38] A. C. Arango, D. C. Oertel, Y. Xu, M. G. Bawendi, V. Bulovic, *Nano Lett.* **2009**, *9*, 860 – 863.
[39] S. Buhbut, S. Itzhakov, E. Tauber, M. Shalom, I. Hod, T. Geiger, Y. Garini, D. Oron, A. Zaban, *ACS Nano* **2010**, *4*, 1293 – 1298.
[40] Y. Li, R. Mastria, K. Li, A. Fiore, Y. Wang, R. Cingolani, L. Manna, G. Gigli, *Appl. Phys. Lett.* **2009**, *95*, 043101 – 043103.
[41] S. Lamansky, P. Djurovich, D. Murphy, F. Abdel-Razzaq, R. Kwong, I. Tsyba, M. Bortz, B. Mui, R. Bau, M. E. Thompson, *Inorg. Chem.* **2001**, *40*, 1704 – 1711.
[42] I. M. Dixon, J. P. Collin, J.-P. Sauvage, L. Flamigni, S. Encinas, F. Barigelletti, *Chem. Soc. Rev.* **2000**, *29*, 385 – 391, and refs. therein.
[43] K. Dedeian, P. I. Djurovich, F. O. Garces, G. Carlson, R. J. Watts, *Inorg. Chem.* **1991**, *30*, 1685 – 1687.
[44] E. A. Plummer, J. W. Hofstraat, L. De Cola, *Dalton Trans.* **2003**, 2080 – 2084.
[45] J. A. Broomhead, C. G. Young, *Inorg. Synth.* **1982**, *21*, 127 – 128.
[46] D. A. Buckingman, F. P. Dwyer, A. M. Sargeson, *Aust. J. Chem.* **1964**, *17*, 622 – 631.
[47] F. P. Dwyer, H. A. Goodwin, E. C. Gyarfas, *Aust. J. Chem.* **1963**, *16*, 42 – 50.
[48] P. A. Lay, A. M. Sargeson, H. Taube, *Inorg. Synth.* **1984**, *24*, 291 – 299.
[49] S. Sprouse, K. A. King, P. J. Spellane, R. J. Watts, *J. Am. Chem. Soc.* **1984**, *106*, 6647 – 6653.
[50] B. P. Sullivan, D. J. Salmon, T. J. Meyer, *Inorg. Chem.* **1978**, *17*, 3334 – 3341.
[51] S. Welter, N. Salluce, P. Belser, M. Groeneveld, L. De Cola, *Coord. Chem. Rev.* **2005**, *249*, 1360 – 1371.
[52] K. Nakamaru, *Bull. Chem. Soc. Jpn.* **1982**, *5*, 1639 – 1640.
[53] F. O. Garces, K. A. King, R. J. Watts, *Inorg. Chem.* **1988**, *27*, 3464 – 3471.
[54] K. Ichimura, T. Kobayashi, K. A. King, R. J. Watts, *J. Phys. Chem.* **2002**, *91*, 6104 – 6106.
[55] F. Lafolet, S. Welter, Z. Popovic, L. De Cola, *J. Mater. Chem.* **2005**, *15*, 2820 – 2828.
[56] K. K.-W. Lo, C.-K. Chung, T. K.-M. Lee, L.-H. Lui, K. H.-K. Tsang, N. Zhu, *Inorg. Chem.* **2003**, *42*, 6886 – 6897.
[57] S. Campagna, F. Puntoriero, F. Nastasi, G. Bergamini, V. Balzani, *Top. Curr. Chem.* **2007**, *280*, 117 – 214.
[58] A. Jurius, V. Balzani, F. Barigelletti, S. Campagna, P. Belser, A. von Zelewsky, *Coord. Chem. Rev.* **1988**, *84*, 85 – 277.
[59] F. Dubois, B. Mahler, B. Dubertret, E. Doris, C. Miosskowski, *J. Am. Chem. Soc.* **2006**, *129*, 482 – 483.
[60] J. R. Lackowicz, *Principles of Fluorescence Spectroscopy*, 3rd ed., Springer, Berlin **2006**, pp. 281 – 282.
[61] D. L. Dexter, *J. Chem. Phys.* **1953**, *21*, 836 – 850.
[62] T. Förster, *Ann. Physik* **1948**, *437*, 55 – 75.
[63] T. Förster, *Fluorezenz Organischer Verbindungen*, Vandenhoeck & Ruprecht, Göttingen, **1951**.
[64] T. Förster, *Discuss. Faraday Soc.* **1959**, *27*, 7 – 17.
[65] Y. Ohsawa, S. Sprouse, K. A. King, M. K. DeArmond, K. W. Hanck, R. J. Watts, *J. Phys. Chem.* **1987**, *91*, 1047 – 1054.
[66] D. A. Buckingham, F. P. Dwyer, A. M. Sargeson, *Inorg. Chem.* **1986**, *5*, 1243 – 1249.
[67] N. Miyaura, K. Yamada, A. Suzuki, *Tetrahedron Lett.* **1979**, *20*, 3437 – 3440.
[68] T. Togano, N. Nagao, M. Tsuchida, H. Kumakura, K. Hisamatsu, F. S. Howell, M. Mukaida, *Inorg. Chim. Acta* **1992**, *195*, 221 – 225.
[69] S. F. Wuister, F. v. Driel, A. Meijerink, *Phys. Chem. Chem. Phys.* **2003**, *5*, 1253 – 1258.
[70] W. W. Yu, L. Qu, W. Guo, X. Peng, *Chem. Mater.* **2003**, *15*, 2854 – 2860.